Available online at www.sciencedirect.com
ScienceDirect
International Journal of Heat and Mass Transfer 51 (2008) 3468–3477
International Journal of HEAT and MASS TRANSFER
www.elsevier.com/locate/ijhmt

Transient natural convection and heat transfer during the storage of granular media

J.G. Avila-Acevedo *, E. Tsotsas

Institute of Process Engineering, Otto-von-Guericke-University, P.O. Box 4120, 39106 Magdeburg, Germany

Received 11 July 2007; received in revised form 5 October 2007
Available online 28 January 2008

Abstract

Transient heat transfer in an originally isothermal cylinder filled with a porous medium after sudden change of wall temperature is studied experimentally and computationally. Lab-scale experiments with water as the interstitial fluid are used in order to imitate the conditions prevailing in large, air-filled industrial silos. The proposed model assumes isotropy of the porous medium, local thermal equilibrium between the phases, Darcy flow and applicability of the Boussinesq approximation. Its predictions are in satisfactory agreement with the experimental results. Simulations reveal the role of dimensionless parameters like the modified porous media Rayleigh number and the cylinder aspect ratio. A criterion for neglecting the influence of natural convection on heat transfer is established.

Keywords: Transient heat transfer; Natural convection; Stored porous media; Silo

1. Introduction

In the production and handling of granular materials like cereals, sugar, salts, polymers, etc., storage is one of the fundamental stages that may seriously affect product quality. Variation of product quality by moisture migration, accumulation of condensed volatile compounds (“silo rain”), caking and even alteration of chemical and microbial stability of the product may occur due to heat and mass transfer taking place when initially warm and slightly moist materials are stored in cold silos or when ambient conditions change [1,2]. Because of these problems, it is important to understand the transport phenomena involved and to investigate the influence of relevant parameters.

As a first step towards a complete treatment of simultaneous heat, mass and momentum transfer, the underlying fundamental problem of transient heat transfer and natural convection will be considered here. Respective simplifications are usual in literature [3]. However, the large majority of previous studies on heat transfer in porous media are related to steady state heat transfer in horizontal, vertical or other cavities (or to the analogous mass transfer problem) with applications to e.g. insulation, aquifers and nuclear reactors (see [4,5] among many others).

The study of transient heat transfer in stored porous media has been addressed mainly in agricultural engineering due to the importance of such phenomena for grain preservation. Mathematical models for the prediction of temperature of silos have been previously developed for one-, two- and three-dimensional cylindrical configurations [3,6]. These works are highly focused on determining temperature distributions for different boundary conditions (i.e. wall materials, solar radiation, wind, etc.). Some of them have assumed negligible effect of natural convection within the medium based on empirical observations (see among others [7]). A first criterion to neglect natural convection is found in [8], where, by an approximate analysis of a mathematical model, grain size and silo aspect ratio are recognized as the main parameters affecting the heat transfer process in stored porous media. In general, transient heat transfer in confined

* Corresponding author. Tel.: +49 391 67 11684; fax: +49 391 67 11160.
E-mail address: juan.avila@st.ovgu.de (J.G. Avila-Acevedo).

0017-9310/$ - see front matter © 2007 Elsevier Ltd. All rights reserved.
doi:10.1016/j.ijheatmasstransfer.2007.10.035

Nomenclature

A	area (m^2)
c	specific heat capacity (J/kg K)
c_P	specific heat capacity of gas at constant pressure (J/kg K)
d	mean particle diameter (m)
g	gravity acceleration (m/s^2)
h	heat transfer coefficient (W/m^2 K)
H	cylinder height (m)
$J_{0,1}$	zeroth- and first-order Bessel function of the first kind
K	permeability (m^2)
k_b	effective bed thermal conductivity (W/m K)
$\dot{Q}$	heat flow rate (J/s)
r	radial coordinate (m)
R	cylinder radius (m)
Ra_b	porous media modified Rayleigh number, Eq. (22)
t	time (s)
T	temperature (°C)
U_0	reference flow velocity (m/s)
v	superficial velocity (m/s)
z	axial coordinate (m)

Greek symbols

α_b	effective bed thermal diffusivity (m^2/s)
α^*	modified bed thermal diffusivity, Eq. (7) (m^2/s)
β	coefficient of thermal expansion (K^{-1})
ΔT	temperature difference (K)
θ	dimensionless temperature
λ_n	eigenvalues
μ	viscosity (kg/m s)
ρ	density (kg/m^3)
σ_b	heat capacity ratio, Eq. (6)
τ	dimensionless time
χ	stream function
ψ	porosity

Indices

avg	averaged
b	bed
f	fluid
r	radial
rel	relative
s	solid
W	wall
z	axial
0	initial, reference
$\wedge$	dimensionless
–	time-averaged

porous media has not yet been intensively studied in literature, although its importance is recognized.

The present work focuses on transient heat transfer in stored porous media in a cylinder cooled at the exterior wall, considering natural convection within the medium. A homogeneous model is derived assuming local thermal equilibrium between the phases and validity of the Darcy law. Analysis of model reveals the parameters influencing the transient heat transfer process. Experiments are performed in packed and water-filled small cylinders, which are a lab-scale analogue for large, air-filled industrial silos. These experiments illustrate the transient behavior of temperature and flow in dependence of relevant model parameters and allow for validation of the model. Additionally, a simulation-based study provides parametric diagrams for the behavior of the system. With the help of this study, a criterion for neglecting natural convection in industrial applications is established.

2. Mathematical model

2.1. System considered

The system under analysis is a cylindrical silo with radius R and height H that is completely filled with a porous medium (Fig. 1). Axial symmetry is assumed and the silo is considered as thermally insulated at top and bottom. The porous medium has initially uniform temperature of T_0. A transient cooling process takes place because the wall temperature is assumed to have a constant and lower value of T_W. Under these conditions heat transfer may be accompanied by convection due to buoyant forces. The aim is to determine the influence of natural convection on the cooling process.

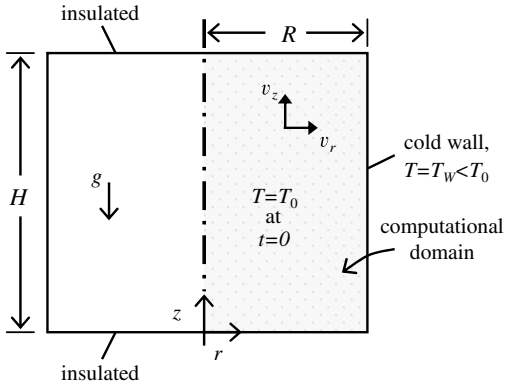

Fig. 1. Scheme of cylindrical silo and computational domain.

2.2. Basic equations

A model for transient heat transfer in a fluid-saturated porous medium is proposed following [9–11]. We assume an isotropic porous medium, thermal equilibrium between the phases (quasi-homogeneous system with single phase flow), negligible heat generation due to the flow and validity of Darcy's law. Considering the physical properties of the solid, of the fluid (viscosity μ, specific heat capacity at constant pressure c_P, coefficient of thermal expansion β) and of the porous medium (permeability K, effective thermal conductivity k_b), the equations expressing the conservation of mass, momentum and energy are

$$\frac{1}{r}\frac{\partial}{\partial r}(rv_r)+\frac{\partial}{\partial z}(v_z)=0, \tag{1}$$

$$\frac{\partial v_r}{\partial z}-\frac{\partial v_z}{\partial r}=-\frac{Kg\rho_0\beta}{\mu}\frac{\partial T}{\partial r}, \tag{2}$$

$$\sigma_b\frac{\partial T}{\partial t}+v_r\frac{\partial T}{\partial r}+v_z\frac{\partial T}{\partial z}=\alpha^*\left[\frac{1}{r}\frac{\partial}{\partial r}\left(r\frac{\partial T}{\partial r}\right)+\frac{\partial^2 T}{\partial z^2}\right], \tag{3}$$

with the following boundary conditions at horizontal walls

$$z=0:\quad v_z=0,\ v_r \text{ free},\ \frac{\partial T}{\partial z}=0, \tag{4a}$$

$$z=H:\quad v_z=0,\ v_r \text{ free},\ \frac{\partial T}{\partial z}=0, \tag{4b}$$

the boundary conditions at the axis and at the vertical wall

$$r=0:\quad v_r=0,\ v_z \text{ free},\ \frac{\partial T}{\partial r}=0 \text{ (symmetry)}, \tag{4c}$$

$$r=R:\quad v_r=0,\ v_z \text{ free},\ T=T_W, \tag{4d}$$

and the initial conditions

$$t=0:\quad v_r=0,\ v_z=0,\ T=T_0. \tag{5}$$

Here, v_r and v_z are the superficial velocities in the radial (r) and axial (z) directions, respectively. Eq. (2) is a combined flow expression obtained by cross differentiation of Darcy's law in r and z directions that helps to avoid pressure calculations [11]. The bed heat capacity ratio σ_b is described by the relationship

$$\sigma_b=\frac{(1-\psi)(\rho c)_s+\psi(\rho c_P)_f}{(\rho c_P)_f}=\frac{(\rho c)_b}{(\rho c_P)_f}. \tag{6}$$

Subscripts s, f and b are referred to solid, fluid and bed. The quantity α^* is the product of the porous medium thermal diffusivity α_b and the bed heat capacity ratio σ_b, according to

$$\alpha^*=\frac{k_b}{(\rho c_P)_f}=\frac{k_b}{(\rho c)_b}\frac{(\rho c)_b}{(\rho c_P)_f}=\alpha_b\sigma_b. \tag{7}$$

As Eq. (2) indicates, the Boussinesq approximation

$$\rho=\rho_0[1-\beta(T-T_0)] \tag{8}$$

has been used, where ρ is the density of fluid at temperature T and ρ_0 is the density of the fluid at a reference temperature equal to the initial temperature T_0. The permeability is related to particle diameter d using the Carman–Kozeny equation [12]

$$K=\frac{d^2\psi^3}{150(1-\psi)^2}, \tag{9}$$

where ψ is the bed porosity.

2.3. Dimensionless problem

For a dimensionless formulation of the problem the following scales are used:

$$\hat{r}=\frac{r}{R},\quad \hat{z}=\frac{z}{H},\quad \theta=\frac{T-T_W}{T_0-T_W}, \tag{10, 11, 12}$$

$$\hat{v}_z=\frac{v_z}{U_0},\quad \hat{v}_r=\frac{H}{R}\frac{v_r}{U_0},\quad \tau=\frac{\alpha^* t}{\sigma_b R^2}. \tag{13, 14, 15}$$

Here, U_0 is the maximal velocity of the fluid attainable for a specific porous medium and temperature difference [13], which can be written as

$$U_0=\frac{Kg\rho_0\beta}{\mu}(T_0-T_W). \tag{16}$$

The transformed model equations are

$$\frac{1}{\hat{r}}\frac{\partial}{\partial\hat{r}}(\hat{r}\hat{v}_r)+\frac{\partial}{\partial\hat{z}}(\hat{v}_z)=0, \tag{17}$$

$$\left(\frac{R}{H}\right)^2\frac{\partial\hat{v}_r}{\partial\hat{z}}-\frac{\partial\hat{v}_z}{\partial\hat{r}}=-\frac{\partial\theta}{\partial\hat{r}}, \tag{18}$$

$$\frac{\partial\theta}{\partial\tau}+Ra_b\left(\frac{R}{H}\right)^2\left[\hat{v}_r\frac{\partial\theta}{\partial\hat{r}}+\hat{v}_z\frac{\partial\theta}{\partial\hat{z}}\right]=\frac{1}{\hat{r}}\frac{\partial}{\partial\hat{r}}\left(\hat{r}\frac{\partial\theta}{\partial\hat{r}}\right)+\left(\frac{R}{H}\right)^2\frac{\partial^2\theta}{\partial\hat{z}^2}, \tag{19}$$

with the boundary conditions at horizontal walls

$$\hat{z}=0,\ \hat{z}=1:\quad \frac{\partial\theta}{\partial\hat{z}}=0,\ \hat{v}_z=0,\ \hat{v}_r \text{ free}, \tag{20a}$$

the boundary conditions at the axis and at the vertical wall

$$\hat{r}=0:\quad \frac{\partial\theta}{\partial\hat{r}}=0,\ \hat{v}_r=0,\ \hat{v}_z \text{ free}, \tag{20b}$$

$$\hat{r}=1:\quad \theta=0,\ \hat{v}_r=0,\ \hat{v}_z \text{ free}, \tag{20c}$$

and the initial conditions

$$\tau=0:\quad \theta=1,\ \hat{v}_r=0,\ \hat{v}_z=0. \tag{21}$$

In these equations two dimensionless groups appear, the square of the cylinder aspect ratio $(R/H)^2$, and the porous medium modified Rayleigh number defined by

$$Ra_b=\frac{Kg\rho_0\beta H}{\mu\alpha^*}(T_0-T_W). \tag{22}$$

Note that for the case of $Ra_b=0$, that is neglecting convection, Eq. (19), reduces to two-dimensional transient conduction in a cylinder. For $R\ll H$ the limiting case of transient conduction in an infinite cylinder is obtained. Eq. (18) represents the potential of fluid movement when a temperature difference is present. Dimensionless velocities have not necessarily a physical meaning. Real velocities

are obtained after multiplying the dimensionless velocities with U_0, Eq. (16), which is a direct function of Ra_b and can be expressed in the form

$$U_0 = \frac{Kg\rho_0\beta}{\mu}(T_0 - T_W) = Ra_b\frac{\alpha^*}{H}. \tag{23}$$

2.4. Potential flow formulation

Before solving the system of Eqs. (17)–(21), it is convenient to introduce a stream function χ, defined by

$$\hat{v}_r = \frac{1}{\hat{r}}\frac{\partial\chi}{\partial\hat{z}}, \quad \hat{v}_z = -\frac{1}{\hat{r}}\frac{\partial\chi}{\partial\hat{r}} \tag{24a, b}$$

[8,14]. It is easy to see that Eqs. (24a,b) automatically satisfy the continuity equation (Eq. (17)). Consequently, the system is reduced to only two partial differential equations for potential flow

$$\left(\frac{R}{H}\right)^2\frac{\partial^2\chi}{\partial\hat{z}^2} + \frac{\partial^2\chi}{\partial\hat{r}^2} - \frac{1}{\hat{r}}\frac{\partial\chi}{\partial\hat{r}} = -\hat{r}\frac{\partial\theta}{\partial\hat{r}}, \tag{25}$$

and for energy

$$\frac{\partial\theta}{\partial\tau} + Ra_b\left(\frac{R}{H}\right)^2\left[\frac{1}{\hat{r}}\frac{\partial\chi}{\partial\hat{z}}\frac{\partial\theta}{\partial\hat{r}} - \frac{1}{\hat{r}}\frac{\partial\chi}{\partial\hat{r}}\frac{\partial\theta}{\partial\hat{z}}\right] = \frac{1}{\hat{r}}\frac{\partial}{\partial\hat{r}}\left(\hat{r}\frac{\partial\theta}{\partial\hat{r}}\right) + \left(\frac{R}{H}\right)^2\frac{\partial^2\theta}{\partial\hat{z}^2}. \tag{26}$$

The respective boundary and initial conditions are

$$\hat{z} = 0: \quad \chi = 0, \ \frac{\partial\theta}{\partial\hat{z}} = 0; \quad \hat{z} = 1: \quad \chi = 0, \ \frac{\partial\theta}{\partial\hat{z}} = 0; \tag{27a}$$

$$\hat{r} = 0: \quad \chi = 0, \ \frac{\partial\theta}{\partial\hat{r}} = 0 \text{ (symmetry)}; \quad \hat{r} = 1: \quad \chi = 0, \ \theta = 0; \tag{27b}$$

$$\tau = 0: \quad \chi = 0, \ \theta = 1. \tag{28}$$

The system of Eqs. (25)–(28) can be solved for θ and χ using an appropriate numerical method.

3. Numerical solution

A finite differences method with central differencing scheme is used for the numerical solution of the problem, including a line-by-line tridiagonal matrix algorithm (TDMA) method for solving the set of algebraic equations obtained after discretizing the potential flow equation, and a Jacobi method for solving the set of algebraic equations after discretizing the energy equation [15,16].

To ensure accuracy and numerical stability, proper spatial and temporal grids must be used. The order of error with the used discretization is $O(\Delta r)^2$, $O(\Delta z)^2$ in space and $O(\Delta\tau)$ in time. Grid independence was checked using grids of different sizes. On this basis, a grid of 80×80 lines was chosen for the present study. The number of time iterations was over 60,000 depending on the values of the parameters.

For additional algorithm verification the already mentioned limiting case of pure conduction in an infinite cylinder ($Ra_b = 0$, $(R/H)^2 \ll 1$) has been considered. The respective analytical solution is

$$\theta(\hat{r},\tau) = 2\sum_{n=1}^{\infty}\frac{J_0(\hat{r}\lambda_n)}{\lambda_n J_1(\lambda_n)}\exp\left(-\lambda_n^2\tau\right) \tag{29a}$$

[17], where the characteristic values λ_n are the roots of the equation

$$J_0(\lambda_n) = 0 \tag{29b}$$

and J_0 and J_1 are the zeroth- and first-order Bessel functions of the first kind, respectively. Analytically and numerically calculated temperature profiles were found to agree within 0.2%.

4. Experimental

Measurements referring to the combined heat transfer and flow problem are not possible in industrial silos for obvious reasons of availability and cost. However, experiments with small packed cylinders are well known from literature [18–20] with the goal of determining the effective thermal conductivity of packed beds. Such an experimental setup is schematically depicted in Fig. 2. It is a jacketed copper cylinder with an internal radius of $R = 19.5$ mm and total height of 265 mm, insulated at top and bottom. In the present work, the cylinder is filled with a bed of glass spheres. It can be heated up and cooled down by water loops through the jacket. Because of high water throughput and the choice of materials, the boundary conditions imposed in this way are very close to a boundary condition of the first kind. This is checked by measuring the temperature at the inlet and outlet of jacket water. The thermal response of the system is captured by recording the temperature in the center of the bed with the help of a thermocouple. The packed height (corresponding to H in Section 2) can be modified by placing additional insulation to the lids of the cylinder.

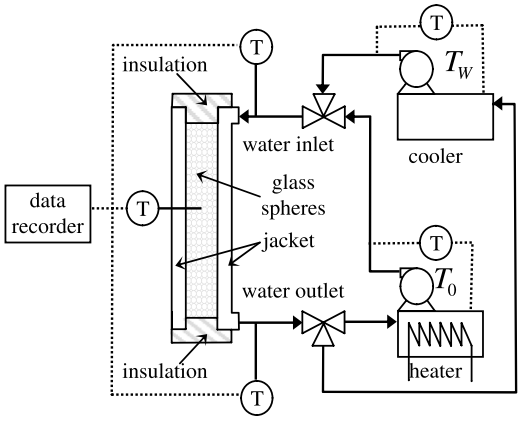

Fig. 2. Experimental setup.

In the experiments, bed temperature was set to the value of $T = T_0$ with the help of the water loop (Fig. 2). Then, the water loop (and consequently also wall temperature) was suddenly switched to a lower temperature $T = T_W$. This starts the cooling process, which is observed until the attainment of thermal equilibrium. In the previous literature, aiming at the determination of quiescent bed thermal conductivity, air was used as the interstitial fluid and the realized temperature difference ($\Delta T = T_0 - T_W$) was small [19,20]. Comparable conditions are listed in the upper part of Table 1. They lead to very small Rayleigh numbers, which correspond to conduction without any significant impact of natural convection.

However, by replacing the interstitial air with water and by increasing the temperature difference, the prevailing conditions change completely; large Rayleigh numbers, as in the lower part of Table 1, are obtained. Such Ra_b-numbers are in the same range as for air-filled industrial-scale silos. Consequently, laboratory measurements in small water-filled packed cylinders can be used for comfortably imitating combined natural convection and heat transfer in industrial silos filled with air or nitrogen, and for validating the model of Section 2.3.

In the course of the present work, apart from the interstitial fluid and the temperature difference, the average diameter of the nearly monodispersed and spherical glass particles and the packed height H (that means the aspect ratio R/H) have also been varied. The ranges of realized experimental parameters are summarized in Table 1, along with the resulting values of Ra_b and $Ra_b(R/H)^2$.

With air as the interstitial fluid at laboratory scale, the same cooling curves ($T(r = 0, z = H/2)$ as function of time) are obtained within experimental accuracy, irrespectively of the precise value of the Rayleigh number. This is in agreement with model results and verifies, on the one hand, the assumption of previous authors about negligible influence of natural convection [18,19]. On the other hand, the effective bed thermal diffusivity of air-glass can be obtained (following [20]) by fitting the analytical solution for pure conduction to the experimental results. This can be transformed to the effective bed thermal conductivity with the help of separately measured bed density and heat capacity (compare with [20]). In the next step, the thermal conductivity of the glass particles can be derived by application of the model of Schlünder, Zehner and Bauer (see [18,21]). Finally, the same model can be applied again to calculate the thermal conductivity (and then the thermal diffusivity) of the water-filled packed bed. In this way, the model can be applied to the water-filled system with high Rayleigh numbers on a completely predictive basis.

Table 1
Experimental parameters

Fluid	R/H	d (mm)	ΔT (K)	Ra_b	$Ra_b(R/H)^2$
Air	0.128	1.82	5	0.05	0.0008
		3.35	5	0.15	0.0025
Water	0.128	1.82	5–50	55–508	0.9–8.3
		3.35	5–50	170–1716	2.8–28.2
	0.193	1.82	5–50	33–336	1.2–12.5
		3.35	5–50	113–1137	4.2–42.3

5. Results and discussion

5.1. Simulations

In Fig. 3 calculated two-dimensional temperature profiles as well as the stream function are presented at different dimensionless times. The case of only conduction ($Ra_b = 0$) is presented in Fig. 3a, where it can be observed how the temperature decreases in radial direction forming straight isotherms that are characteristic for one-dimensional heat transfer. As soon as the temperature gradient appears, the potential of fluid movement is also present, but because real velocities are obtained using Eqs. (13) and (14), they become zero and no movement of fluid exists.

In Figs. 3b and 4a, the effect of natural convection is considered for the aspect ratio 0.128 at two different flow intensities, $Ra_b = 1700$ and 680, respectively. Opposite to the conduction case, the isotherms are not longer straight and vertical. The profile is distorted because the fluid is moving inside the bed. The fluid carries heat towards the upper part of the non-insulated wall, therefore a lower temperature is observed in the lower part of the bed. By comparing both figures, it is clear that the changes of both temperature profile and flow pattern inside the cylinder become stronger with the increase of Ra_b, the latter being the main parameter influencing natural convection. Note that the values of the stream function are negative, which represents a clockwise flow.

The effect of aspect ratio is observed in Fig. 4, where temperature profiles and stream function are depicted keeping constant the Rayleigh number. A faster temperature decrease for the case of the short cylinder ($R/H = 0.193$) shown in Fig. 4b in comparison with the tall cylinder ($R/H = 0.128$) in Fig. 4a, reveals that the aspect ratio also influences natural convection. It is worth to note that the aspect ratio not only affects flow intensity but also slightly modifies the flow pattern, stretching it for taller cylinders.

5.2. Comparison of simulations with experiments

Transient temperatures measured in the middle of the cylinder are compared in dimensionless form with numerical results in Fig. 5. For the limiting case of $Ra_b = 0$ only computed results are plotted. As already explained, these correspond to the measurements with air (Table 1). All experimental results presented in Fig. 5 have been gained with water and $Ra_b \geqslant 55$. Variations on Rayleigh number are attained, according to Table 1, by changing either the temperature difference, the particle size or the cylinder height. Increasing the temperature difference results in a larger Rayleigh number according to Eq. (22). Conse-

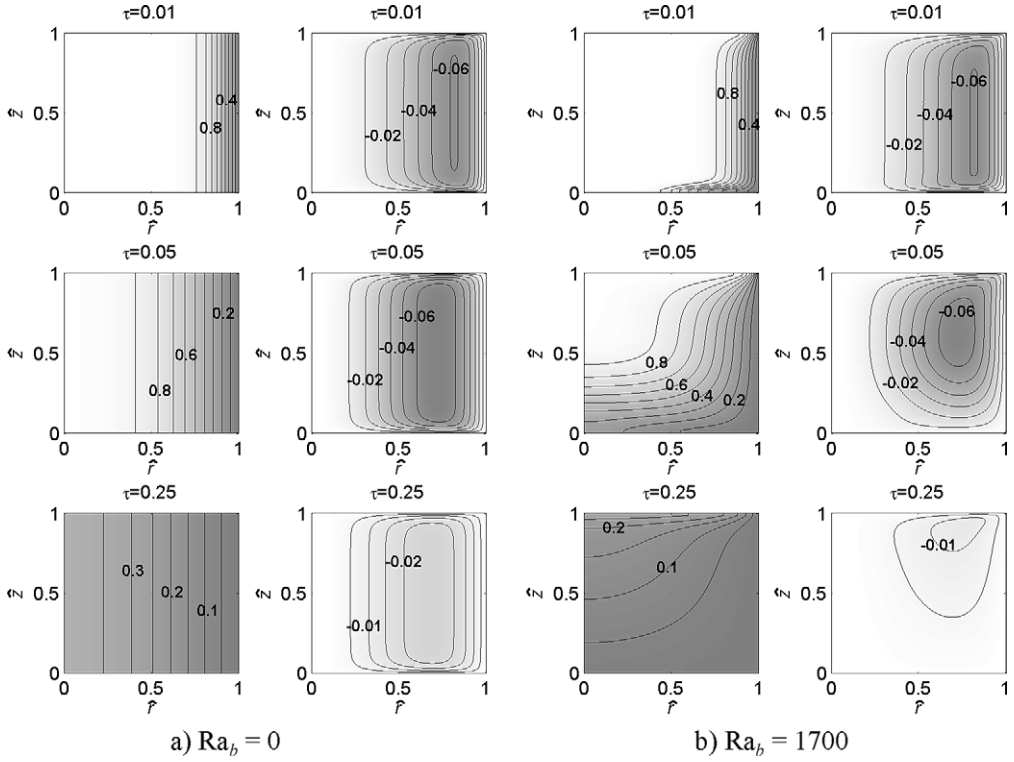

Fig. 3. Transient temperature profiles and stream function for $R/H = 0.128$.

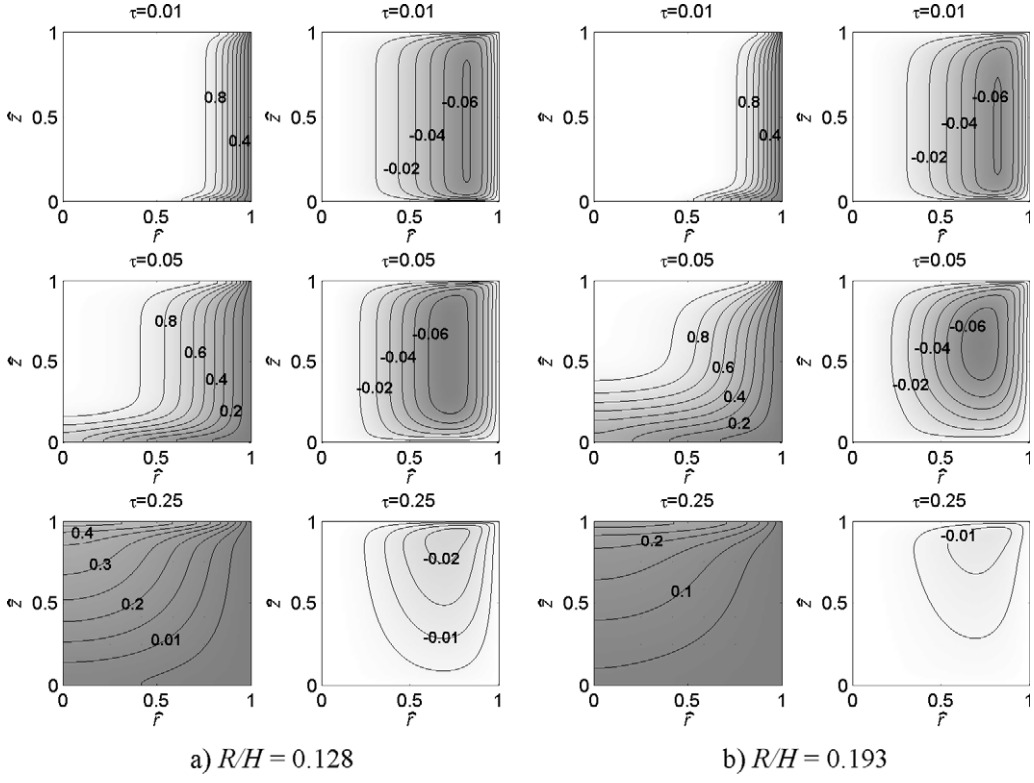

Fig. 4. Transient temperature profiles and stream function for $Ra_b = 680$.

quently, a stronger effect of natural convection is observed (Fig. 5a–c). A similar variation is noticed when particle size (and therefore bed permeability) is increased, as it can be seen by comparing Fig. 5b with Fig. 5a. The Rayleigh num-

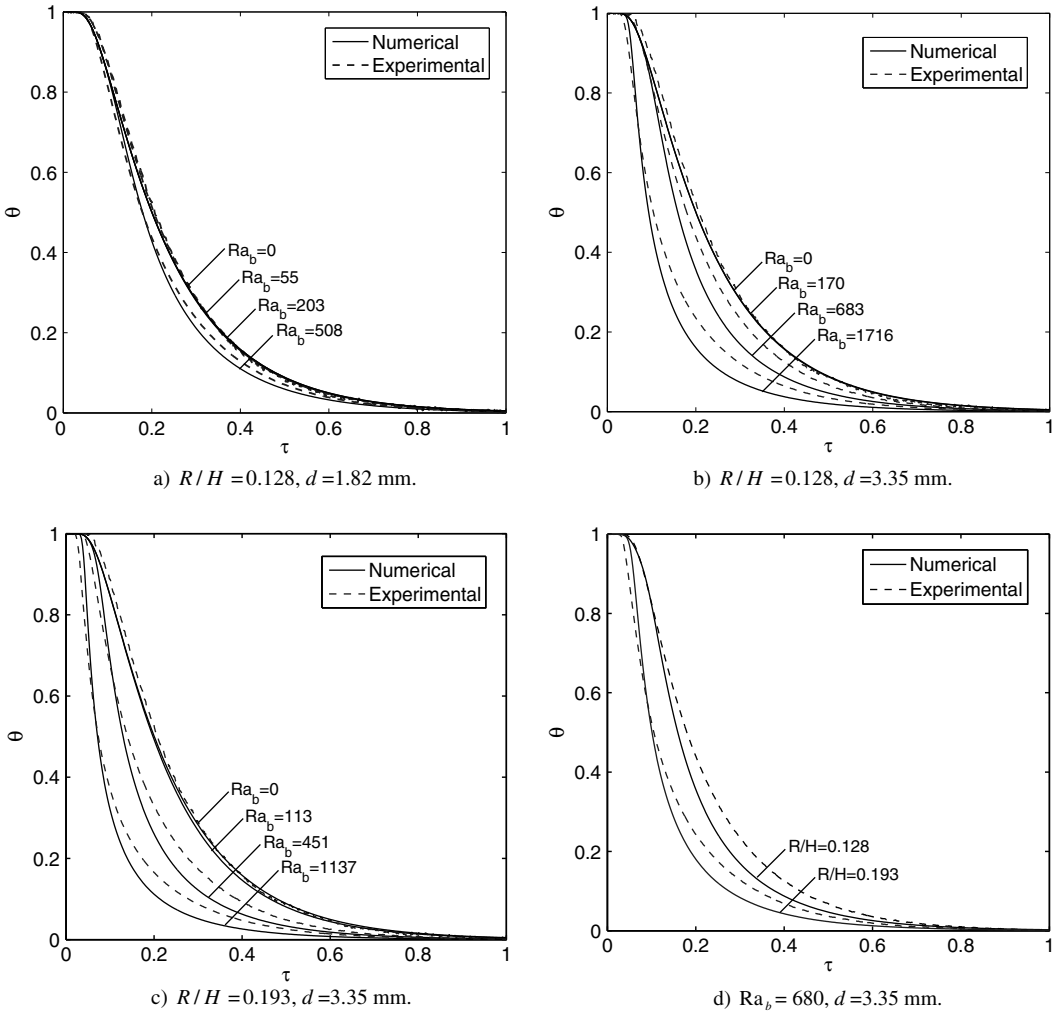

a) $R/H = 0.128$, $d = 1.82$ mm.

b) $R/H = 0.128$, $d = 3.35$ mm.

c) $R/H = 0.193$, $d = 3.35$ mm.

d) $Ra_b = 680$, $d = 3.35$ mm.

Fig. 5. Comparison between numerical and experimental results.

ber is also influenced by the cylinder height, as shown by Fig. 5b and c. Data on these Figures have been gained with the same particle size and the same temperature differences, but with different bed heights.

As predicted by the theory for given temperature difference, particle size and cylinder height, the curves for low Rayleigh numbers are close to the limit of pure conduction. Heat transfer is significantly enhanced at large values of the Rayleigh number. Consequently, the Rayleigh number may have a large influence on the process.

The influence of the aspect ratio at constant Rayleigh number is presented in Fig. 5d. By observing the dimensionless center temperature it is found that the cooling rate increases for larger aspect ratios. The influence of this second parameter, as for the case of Rayleigh number, is experimentally verified.

In general, the agreement between model predictions and experimental results is good, validating the model from Section 2 of this work. Small deviations, which can still be observed between simulations and experiment in Fig. 5, are probably due to the influence of the cylinder wall. It is planned to upgrade the model in the near future by taking into account the increase of bed porosity and flow in the immediate vicinity of the walls. Such an upgrade is expected to further improve the agreement between simulation and lab-scale experiments. However, it will not be significant for the case of large industrial silos.

Once the parameters affecting natural convection have been analyzed separately, it is worth to look again at the equation where these parameters appear. Eq. (19) suggests that the convective term is not influenced by the Rayleigh number or by the aspect ratio separately, but by the product $Ra_b(R/H)^2$. By plotting the transient of dimensionless center temperature considering this combined parameter, it is found that similar values of $Ra_b(R/H)^2$, which can be reached by modifying either Ra_b or R/H, have the same influence on the cooling process. This is exemplified in Fig. 6, where the value of, e.g., $Ra_b(R/H)^2 = 5$ can be reached with $Ra_b = 300$ in the case of the taller cylinder or with $Ra_b = 134$ for the shorter. For the sake of clarity, we have refrained from plotting simulation results in Fig. 6.

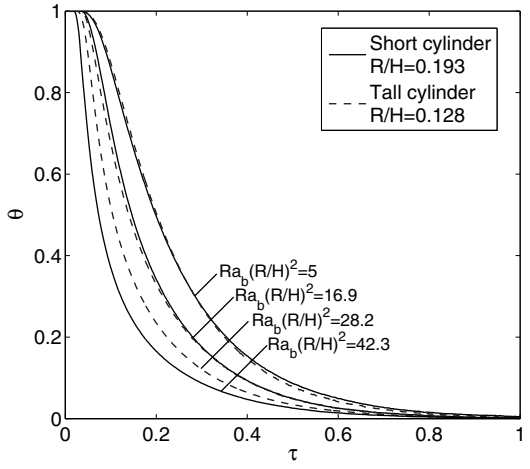

Fig. 6. Effect of $Ra_b(R/H)^2$ on the cooling process.

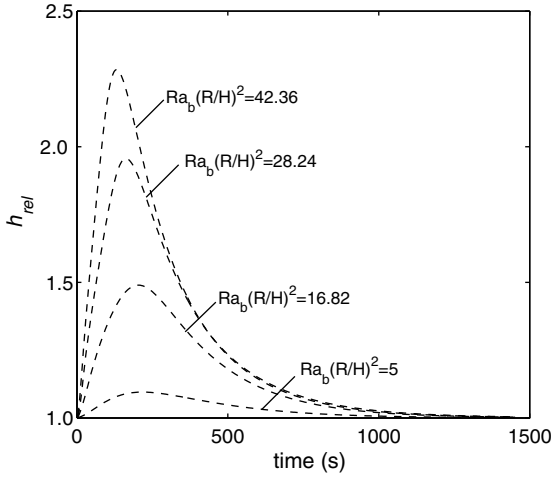

Fig. 7. Dependence of relative heat transfer coefficient on $Ra_b(R/H)^2$.

5.3. Influence of convection on heat transfer

The dependence of Nusselt number on Rayleigh number is well known for several cases of steady state heat transfer [5]. For the present problem of transient heat transfer the use of a relative heat transfer coefficient is proposed according to

$$h_{rel} = \frac{h_{avg}(\text{condution} + \text{convection})}{h_{avg}(\text{only conduction})}. \tag{30}$$

The heat transfer coefficients at the right-hand side of Eq. (30) are based on average quantities over space as follows

$$h_{avg} = \frac{\dot{Q}}{A(T_{avg} - T_W)}; \tag{31}$$

$\dot{Q}$ is the total heat flow rate transferred out of the cylinder, T_{avg} is the average temperature in the cylinder and A is the non-adiabatic cylinder surface area. However, the coefficients h_{avg} as well as the relative heat transfer coefficient h_{rel} are time dependent. A time-averaged value that allows to easily identify the effect of parameters on the process can be defined as

$$\bar{h}_{rel} = \int h_{rel}\, d\tau. \tag{32}$$

The influence of the parameter $Ra_b(R/H)^2$ on the transient behavior of the relative heat transfer coefficient is presented in Fig. 7. From this figure it can be recognized on one hand that, the higher the value of $Ra_b(R/H)^2$, the larger is the deviation from the conduction case ($h_{rel} > 1$). On the other hand, the time dependency of the relative heat transfer coefficient is clearly observed, suggesting the way the heat is transported: heat conduction is always present, being the dominating mechanism at the beginning. As soon as a significant temperature gradient has evolved, natural convection appears and grows, reaching a maximum when the cooling front has penetrated to the center of the cylinder. From that point on, natural convection decreases. At final stages, both conduction and convection disappear.

By considering time-averaged coefficients (from $\tau = 0$–1), parametric diagrams as those of Fig. 8 can be obtained. In Fig. 8a, curves of equal time-averaged coefficient are plotted as functions of the square of the aspect ratio and of Rayleigh number. It can be recognized that for large aspect ratios (short cylinders), natural convection is significant even at low Rayleigh numbers. For the case of tall cylinder, an equivalent effect of natural convection is achieved only when Rayleigh numbers are considerably larger. A reasonable criterion for the significance of natural convection can be defined by a contribution of this mechanism to heat transfer by more than 5%. Consequently, natural convection can be neglected in the region under the curve corresponding to the $\bar{h}_{rel} = 1.05$ in Fig. 8a.

In Fig. 8b lines of equal time-averaged heat transfer coefficient are plotted considering the product $Ra_b(R/H)^2$, which is the main parameter expressing the influence of natural convection on heat transfer, as the ordinate. This offers a complete view of the parameters in Eqs. (17)–(21). On one side, for large values of $Ra_b(R/H)^2$ natural convection is found to be slightly dependent on the aspect ratio. This dependency can be explained by observing that modifying the aspect ratio, the convective heat transport will be affected because of the change of dimensionless velocities in Eq. (18). On the other side, for small values of $Ra_b(R/H)^2$ the convective contribution can be considered as independent from the aspect ratio. Therefore, the region where the effect of natural convection can be neglected is now under a straight line. The criterion for neglecting the contribution of natural convection (<5%) to heat transfer becomes

$$Ra_b(R/H)^2 < 10, \tag{33}$$

with the side-condition

$$0.06 < R/H < 0.3. \tag{34}$$

This latter condition just reflects the range of simulations conducted in the present work.

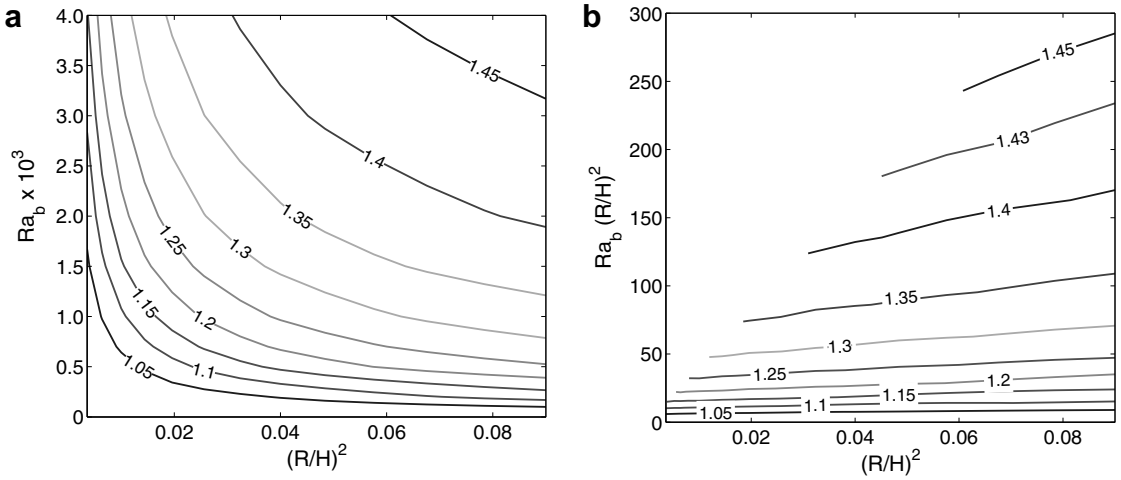

Fig. 8. Time-averaged relative heat transfer coefficients as functions of the main parameters of the problem.

This result differs from that proposed in [8], where a criterion is derived only by mathematical analysis of model equations. The criterion form [8] is a complex function depending not only on the Rayleigh number (based on the effective bed thermal conductivity) and the aspect ratio, but also on the heat capacity ratio as a third parameter. It overestimates the effect of natural convection for small aspect ratios. In contrast, the criterion proposed in the present work is based on the numerical solution and is additionally corroborated by experiments. Consequently, it may be expected to be accurate for a range of aspect ratios that covers most of the industrial silos.

6. Conclusions

The transient heat transfer in an originally isothermal cylinder filled with a porous medium after sudden exposure to a cold environment is considered in this paper. Dimensionless expression of the mathematical model shows that the most important parameters affecting natural convection are the porous media modified Rayleigh number and the cylinder aspect ratio. The dependence of the influence of natural convection on heat transfer from such parameters has been studied experimentally and by simulations. Natural convection has been found to have a very small influence on heat transfer in small cylinders filled with particles and air, as frequently used in the laboratory for the determination of packed bed thermal conductivity. However, it may have a strong influence in large industrial silos. A similar influence is obtained at the laboratory scale by exchanging the air with water. Numerical solution of the problem shows a good agreement between model predictions and measurements. Furthermore, the numerical analysis reveals details of the transient behavior of natural convection. The influence of natural convection increases rapidly after the onset of the cooling process and reaches a maximum, before decreasing gradually and disappearing. In the average, natural convection contributes by more than 5% to the heat transfer if the relationship $Ra_b(R/H)^2 > 10$ is fulfilled. Consequently, non-fulfillment of this relationship can be used as a criterion for neglecting natural convection in practical applications.

Acknowledgements

The first author gratefully acknowledges the financial support by the Deutscher Akademischer Austauschdienst (DAAD) and the Consejo Nacional de Ciencia y Tecnología (CONACyT) México.

References

[1] A. Lacey, M.P. Søresen, Danisco: temperature and moisture gradients in sugar silos, in: 32nd European Study Group with Industry, Final Report, Technical University of Denmark, 1998, pp. 37–46.
[2] M. Schneider, E. Tsotsas, On the predictability of silo rain: modeling moisture migration in beds of particulates after drying, in: Proceedings of the First Nordic Drying Conference, Trondheim, Norway, 2001, Paper No. 15.
[3] D.S. Jayas, N.D.G. White, W.E. Muir, Stored Grain Ecosystems, Marcel Dekker Inc., New York, 1995.
[4] J. Bear, A. Verruijt, Modeling Ground Water Flow and Pollution, D. Reidel Publishing Co., Holland, 1987.
[5] D.A. Nield, A. Bejan, Convection in Porous Media, second ed., Springer-Verlag, New York, 1999.
[6] M.E. Casada, J.H. Young, Model for heat and moisture transfer in arbitrarily shaped two-dimensional porous media, Trans. ASAE 37 (6) (1994) 1927–1938.
[7] K. Alagusundaram, D.S. Jayas, N.D.G. White, W.E. Muir, Finite difference model of three-dimensional heat transfer in grain bins, Can Agric Eng 32 (1990) 315–321.
[8] E.A. Smith, S. Sokhansanj, Natural convection and temperature of stored produce – a theoretical analysis, Can Agric Eng 32 (1989) 91–97.
[9] L. Burmeister, Convective Heat Transfer, second ed., John Wiley & Sons Inc., 1993.
[10] U. Hornung, Homogenization and Porous Media, Springer-Verlag, New York, 1997.
[11] A. Bejan, Convection Heat Transfer, second ed., Wiley, New York, 1995.
[12] E.-U. Schlünder, E. Tsotsas, Wärmeübertragung in Festbetten, durchmischten Schüttgütern und Wirbelschichten, Thieme Verlag, Stuttgart-New York, 1988.

[13] A. Nakayama, PC-Aided Numerical Heat Transfer and Convective Flow, CRC Press Inc., London, 1995.
[14] E. Holzbecher, Modeling Density-Driven Flow in Porous Media, Springer-Verlag, Berlin, 1998.
[15] M.N. Ozisik, Finite Difference Methods in Heat Transfer, CRC Press, Florida, 1994.
[16] K. Muralidhar, T. Sundararajan, Computational Fluid Flow and Heat Transfer, Narosa Publishing House, New Delhi, 1995.
[17] H.S. Carslaw, J.C. Jaeger, Conduction of Heat in Solids, second ed., Clarendon Press, Oxford, 1959.
[18] E. Tsotsas, H. Martin, Thermal conductivity of packed beds: A review, Chem Eng Process 22 (1987) 19–37.
[19] E. Tsotsas, E.-U. Schlünder, Impact of particle size dispersity on thermal conductivity of packed beds: measurement, numerical simulation, prediction, Chem Eng Technol 14 (1991) 421–427.
[20] W. Kwapinski, E. Tsotsas, Characterization of particulate materials in respect to drying, Drying Technol 24 (2006) 1083–1092.
[21] E. Tsotsas, Section Deb in VDi-Waermeatlas, ninth ed., Springer-Verlag, Berlin, 2002.